

PAPER

# Long-term stability of intracortical recordings using perforated and arrayed Parylene sheath electrodes

To cite this article: Seth A Hara *et al* 2016 *J. Neural Eng.* **13** 066020

View the [article online](#) for updates and enhancements.

## Related content

- [3D Parylene sheath neural probe for chronic recordings](#)  
B J Kim, J T W Kuo, S A Hara *et al.*
- [Acute in vivo testing of a conformal polymer microelectrode array for multi-region hippocampal recordings](#)  
Huijing Xu, Ahuva Weltman Hirschberg, Kee Scholten *et al.*
- [Progress towards biocompatible intracortical microelectrodes for neural interfacing applications](#)  
Mehdi Jorfi, John L Skousen, Christoph Weder *et al.*

## Recent citations

- [Recent Progress on Non-Conventional Microfabricated Probes for the Chronic Recording of Cortical Neural Activity](#)  
Chaebin Kim *et al*
- [From softening polymers to multimaterial based bioelectronic devices](#)  
Melanie Ecker *et al*
- [Characterization and Modification of Adhesion in Dry and Wet Environments in Thin-Film Parylene Systems](#)  
Jessica Ortigoza-Diaz *et al*



The Department of Bioengineering at the University of Pittsburgh Swanson School of Engineering invites applications from accomplished individuals with a PhD or equivalent degree in bioengineering, biomedical engineering, or closely related disciplines for an open-rank, tenured/tenure-stream faculty position. We wish to recruit an individual with strong research accomplishments in Translational Bioengineering (i.e., leveraging basic science and engineering knowledge to develop innovative, translatable solutions impacting clinical practice and healthcare), with preference given to research focus on neuro-technologies, imaging, cardiovascular devices, and biomimetic and biorobotic design. It is expected that this individual will complement our current strengths in biomechanics, bioimaging, molecular, cellular, and systems engineering, medical product engineering, neural engineering, and tissue engineering and regenerative medicine. In addition, candidates must be committed to contributing to high quality education of a diverse student body at both the undergraduate and graduate levels.

[CLICK HERE FOR FURTHER DETAILS](#)

**To ensure full consideration, applications must be received by June 30, 2019. However, applications will be reviewed as they are received. Early submission is highly encouraged.**

# Long-term stability of intracortical recordings using perforated and arrayed Parylene sheath electrodes

Seth A Hara<sup>1,3</sup>, Brian J Kim<sup>1</sup>, Jonathan T W Kuo<sup>1,4,5</sup>, Curtis D Lee<sup>1</sup>, Ellis Meng<sup>1</sup> and Victor Pikov<sup>2,6</sup>

<sup>1</sup>Department of Biomedical Engineering, University of Southern California, Los Angeles, CA, USA

<sup>2</sup>Neural Engineering Program, Huntington Medical Research Institutes, Pasadena, CA, USA

E-mail: [ellis.meng@usc.edu](mailto:ellis.meng@usc.edu).

Received 15 September 2016

Accepted for publication 10 October 2016

Published 7 November 2016



CrossMark

## Abstract

**Objective.** Acquisition of reliable and robust neural recordings with intracortical neural probes is a persistent challenge in the field of neuroprosthetics. We developed a multielectrode array technology to address chronic intracortical recording reliability and present *in vivo* recording results. **Approach.** The  $2 \times 2$  Parylene sheath electrode array (PSEA) was microfabricated and constructed from only Parylene C and platinum. The probe includes a novel three-dimensional sheath structure, perforations, and bioactive coatings that improve tissue integration and manage immune response. Coatings were applied using a sequential dip-coating method that provided coverage over the entire probe surface and interior of the sheath structure. A sharp probe tip taper facilitated insertion with minimal trauma. Fabricated probes were subject to examination by optical and electron microscopy and electrochemical testing prior to implantation. **Main results.**  $1 \times 2$  arrays were successfully fabricated on wafer and then packaged together to produce  $2 \times 2$  arrays. Then, probes having electrode sites with adequate electrochemical properties were selected. A subset of arrays was treated with bioactive coatings to encourage neuronal growth and suppress inflammation and another subset of arrays was implanted in conjunction with a virally mediated expression of Caveolin-1. Arrays were attached to a custom-made insertion shuttle to facilitate precise insertion into the rat motor cortex. Stable electrophysiological recordings were obtained during the period of implantation up to 12 months.

Immunohistochemical evaluation of cortical tissue around individual probes indicated a strong correlation between the electrophysiological performance of the probes and histologically observable proximity of neurons and dendritic sprouting. **Significance.** The PSEA demonstrates the scalability of sheath electrode technology and provides higher electrode count and density to access a greater volume for recording. This study provided support for the importance of creating a supportive biological environment around the probes to promote the long-term electrophysiological performance of flexible probes in the cerebral cortex. In particular, we demonstrated beneficial effects of the Matrigel coating and the long-term expression of Caveolin-1. Furthermore, we provided support to an idea of using an artificial acellular tissue compartment as a way to counteract the walling-off effect of the astrocytic scar formation around

<sup>3</sup> Present address: Mayo Clinic, Rochester, MN, USA.

<sup>4</sup> Present address: The United States Patent and Trademark Office, San Jose, CA, USA.

<sup>5</sup> The views and opinions expressed in this article are the author's personal views and opinions and do not necessarily represent the views of either the United States Patent and Trademark Office or the United States Government.

<sup>6</sup> Present address: Galvani Bioelectronics, Stevenage, UK.

the probes as a means of establishing a more intimate and stable neural interface.

**Keywords:** Parylene, intracortical electrode array, brain–machine interfaces, microelectrode array, chronic implants, dendrite sprouting, neural interface

(Some figures may appear in colour only in the online journal)

## 1. Introduction

Recording of consistent, dependable intracortical neural signals remains a challenge in the field of neuroprosthetics. The chronic immune response, which results in retraction of dendritic processes, neuronal cell death, and glial encapsulation [1–5], remains a significant barrier despite many countermeasures that have been attempted. Strategies include direct modulation of brain's immune response and dendritic outgrowth through bioactive molecules, indirect mitigation of the immune response through novel neural probe design, and combinations of the above strategies.

Bioactive molecules have been shown to effectively attract dendritic processes closer to the probe's recording sites to improve recording quality. This has been demonstrated both by encouraging dendritic attachment to the probe [6, 7] and by suppressing the astrocytic adhesion to the probe to indirectly promote the reach of dendritic processes through the probe-bound layer of astrocytes [8]. Other approaches seek to curtail the immune response and prevent the activation of astrocytes and microglia, thereby inhibiting the formation of a glial sheath [9–13].

Neural probe geometry also affects glial encapsulation and activation of the immune response. Skousen *et al* proposed that an open-architecture probe can reduce microglial activation and the impact of the resulting released chemical factors that promote inflammation and reduce neuronal apoptosis [14]. These results corroborate the conclusions of Seymour and Kipke that open-architecture probes can increase tissue integration, reduce adhesion of reactive cells, and improve cell-to-cell communication through increased diffusion of chemical factors in local tissue [15].

A large body of work has been dedicated to fabricating neural probes from materials that more closely mimic the mechanical properties of brain tissue. The mechanical mismatch between conventional neural probe materials (metal microwires, silicon, and ceramic) with a Young's modulus of 100–400 GPa and brain tissue with a Young's modulus of 0.4–6 kPa [16] coupled with the micromotion arising from vascular and respiratory oscillations further aggravate the immune response and lead to chronic inflammation [3, 17–21]. To address these concerns, neural probes based on flexible substrates with reduced Young's moduli have been developed to better match the soft mechanical properties of the brain.

Although thin film silicon has been utilized as a flexible substrate [22], most efforts employ polymer substrates that are less susceptible to breakage, such as polyimide [23–25], Parylene C [26–29], or SU-8 [30]. Polyimide, Parylene, and SU-8, with Young's moduli of ~3 GPa [18, 31], 2.7–3.7 GPa [32], and 2 GPa [33], respectively, provide two orders of

magnitude reduction in substrate stiffness over conventional substrate materials (e.g. silicon). However, unlike polyimide and Parylene, SU-8 does not have a history of use in Food and Drug Administration approved medical implants.

The neurotrophic electrode (NE) developed by Kennedy combines an open-architecture design with the use of growth factors to actively stimulate dendritic outgrowth toward the recording sites in the probe interior [34, 35]. This combined use of bioactive molecules and novel open-architecture probe design successfully anchored the probe into the tissue and provided stable recordings for over four years in humans [36]. Nonetheless, the NE is manually fabricated from microwires and a pulled glass micropipette tip. Although a promising technology, it does not lend itself to batch manufacturing nor include a strategy to reduce the mechanical mismatch.

Previously we developed a flexible intracortical neural probe using Parylene C (hereto referred to as Parylene), a United States Pharmacopeia Class VI polymer with a long history of use in medical implants for its desirable properties, as a structural material. Only Parylene and platinum were used in the manufacture of the three-dimensional (3D) Parylene sheath electrode (PSE) via highly repeatable batch fabrication techniques. Furthermore, the NE approach to integrate bioactive coatings was adapted for the sheath to promote neuronal growth and mitigate the immune response. The potential of the PSE was initially demonstrated in a successful one month study in the rat [37].

In this work, the PSE technology was further improved to produce the Parylene Sheath Electrode Array (PSEA) comprising a  $2 \times 2$  array with 32 total electrodes (eight on each PSE). The probe tip was redesigned to minimize footprint and increase taper to facilitate implantation and attempt to minimize the immune response. Perforations through the sheath were added to provide a more open architecture facilitating cell-cell and fluid communication as well as tissue integration. Individual  $1 \times 2$  arrays were assembled using a precision stacking technique to achieve  $2 \times 2$  arrays and to demonstrate the possibility of achieving even larger arrays. A new coating methodology was developed to simultaneously apply a bioactive molecule cocktail to the entire surface of all probes in the array. Additionally, we investigated an alternate approach using bare, uncoated probes in a rat brain pre-treated with microinjections of a viral construct, AAV9-SynCav1, designed to promote neuronal survival and growth [38]. A new insertion shuttle was designed and fabricated that allows simultaneous placement of the four individual PSEs. Successful recording of neural signals *in vivo* was obtained for up to 12 months, demonstrating the scalability of this technology and the potential for tight tissue integration with Parylene-based neural probes.

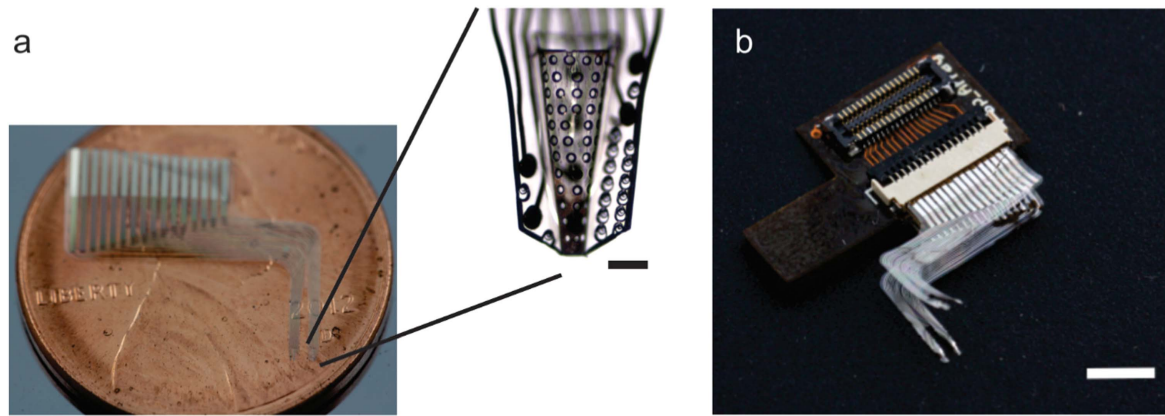


**Figure 1.** Images of a  $1 \times 2$  array with close-up of a sheath structure showing placement of four electrodes inside of sheath and four on the periphery, scale bar =  $100 \mu\text{m}$  (a) and fully packaged  $2 \times 2$  PSEA, scale bar = 5 mm (b).

## 2. Materials and methods

### 2.1. Design and fabrication

Each sheath of the PSEA tapered from  $300$  to  $50 \mu\text{m}$  and contained eight platinum electrodes with an exposed area  $45 \mu\text{m}$  in diameter. Four electrodes were positioned inside of the sheath and four on the periphery of the probe (figure 1(a)).  $1 \times 2$  sheath arrays were fabricated with mirror-image layouts on wafer with the sheaths positioned 1 mm apart, center to center. The  $1 \times 2$  arrays were packaged back-to-back in pairs, resulting in a  $2 \times 2$  PSEA with a total of 32 electrodes (figure 1(b)). The probe tip geometry of the PSEA was improved based on observations from our previous study to reduce insertion trauma and inflammation [37]. As such, the tip was designed with a sharper taper to aid insertion and minimize the penetration profile. In an effort to facilitate chemical diffusion for cell-to-cell communication and to minimize probe surface area,  $15 \mu\text{m}$  diameter perforations were created throughout the entire probe tip and the fabrication process [28] was revised to accommodate the patterning of these additional features.

Perforations were designed to be  $15 \mu\text{m}$  in diameter and spaced at least  $10 \mu\text{m}$  from each other in order to maintain the structural integrity of the Parylene sheath while providing sufficient clearance for dendritic processes to pass through. Eighty perforations were made on each probe, positioned along the bottommost  $800 \mu\text{m}$  of the probe both within the sheath periphery (16 perforations) and within the sheath structure (54 perforations), as seen in figure 1(a).

A brief summary of the modified fabrication process for including perforations is as follows. The PSEA was fabricated through surface micromachining of Parylene and thin film platinum. Platinum was chosen for electrode sites and traces as it is an inert, biocompatible metal commonly used for neural interfaces. To begin, a  $5 \mu\text{m}$  layer of Parylene was deposited on a silicon carrier wafer with its native oxide intact through a room-temperature chemical vapor deposition process. Photoresist was applied in preparation for metal lift-off, thin film platinum for electrode sites and traces was electron beam deposited, and metal patterns were revealed by lift-off

in acetone followed by successive rinses in isopropyl alcohol and deionized water. A  $2 \mu\text{m}$  Parylene insulation layer was deposited over the metal layer (figure 2(a)) and electrode sites, contact pads, and perforations in the substrate were exposed using oxygen plasma reactive ion etching (figure 2(b)). A photoresist sacrificial structure was patterned (figure 2(c)) and coated with a  $5 \mu\text{m}$  Parylene layer to form a trapezoidal microchannel. Once more, electrode sites, contact pads, and perforations were re-exposed using oxygen plasma reactive ion etching (figure 2(d)). At the same time, access ports on both ends of the microchannel were also etched. Finally, the outline of the  $1 \times 2$  arrays was etched out and arrays were released from the carrier wafer. The sacrificial photoresist in the microchannel was removed through an acetone soak (figure 2(e)) and the PSEAs were rinsed in acetone, isopropyl alcohol, and deionized water before they were left to air dry.

To create the final 3D sheath structure from the microchannel (figure 3(a)), a thermal molding process was used to impart the shape change. A custom-tapered stainless steel microwire was manually inserted into the  $300 \mu\text{m}$  access port, temporarily opening the sheath into a conical shape (figure 3(b)). With the microwire in place, the assembly was heated to  $200^\circ\text{C}$  in a vacuum oven for 48 h and then slowly cooled back to room temperature to induce the shape change from a flat to a 3D sheath without thermal oxidation. The microwire was then removed (figure 3(c)).

### 2.2. Packaging

Once thermoforming was complete, the  $1 \times 2$  arrays were connected to a flexible printed circuit (FPC) with a 16-channel zero-insertion-force (ZIF) connector. A polyetheretherketone (PEEK) backing was applied to the contact pad area of the array to provide the necessary stiffness and thickness to insert the  $1 \times 2$  arrays into the ZIF and engage the closing latch. Two  $1 \times 2$  arrays were connected back-to-back onto a single double-sided FPC to create a  $2 \times 2$  PSEA (figure 4). A BM10 connector (Hirose Electric Co., Ltd, Tokyo, Japan) was used to connect the PSEA to an adapter (figure 5) for reversible connections to the Omnetics

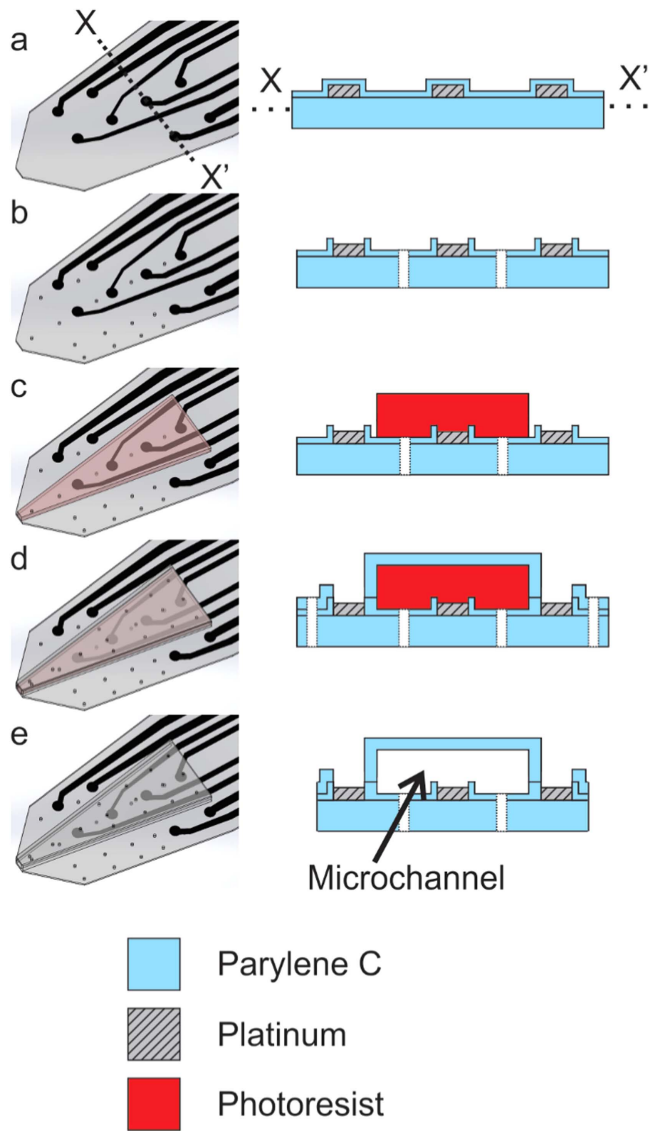


**Figure 2.** Overview of the fabrication process of the PSEA with cross-section. Only the outline of a sheath is shown for clarity in the three dimensional images on the left side. Metal electrodes and traces were patterned and insulated with Parylene (a). Contact pads and perforations were etched with  $O_2$  plasma in a reactive ion etcher (RIE) (b). A photoresist sacrificial layer was patterned (c). Parylene was deposited on the sacrificial layer and contact pads and perforations were etched with  $O_2$  RIE (d). Once released, the sacrificial layer was removed to form a flat microchannel (e).

connector on the data acquisition system (OmniPlex; Plexon Inc., Dallas, TX).

### 2.3. In vitro testing

**2.3.1. Electrochemical testing.** Prior to implantation, benchtop testing was conducted to characterize the electrochemical (EC) performance of the PSEA. All EC testing was conducted with a Reference 600 potentiostat (Gamry Instruments, Warminster, PA) with a three-electrode setup, utilizing a  $1\text{ mm}^2$  Pt wire counter electrode and Ag/AgCl (3 M NaCl) reference electrode (BASi, West Lafayette, IN). A Faraday cage was used to minimize external noise.

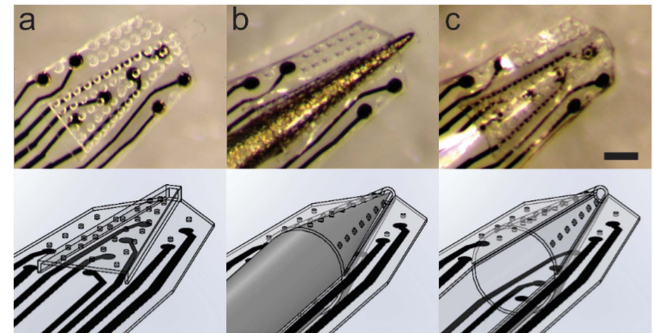


**Figure 3.** Optical micrographs and schematics depicting the thermoforming process. Sheath structures are flat as fabricated on the wafer (a). A custom-tapered microwire is inserted into the sheath, mechanically opening it and serving as a mold for the thermoforming (b). Following annealing, the microwire is removed and the sheath retains its shape (c). Scale bar =  $100\ \mu\text{m}$ .

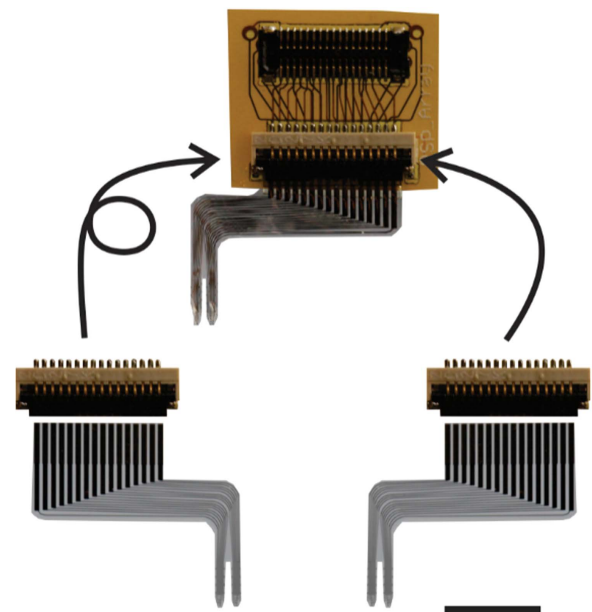


**Figure 4.** Diagram showing the  $2 \times 2$  packaging scheme.  $1 \times 2$  arrays are inserted into ZIF connectors and then placed back-to-back on a FPC. Scale bar = 5 mm.

Cyclic voltammetry was performed to electrochemically clean the electrode surfaces prior to further testing (immersion in  $0.05\text{ M H}_2\text{SO}_4$  and 30 cycles from  $-0.2$  to  $1.2\text{ V}$  versus Ag/AgCl (3 M NaCl) at a scan rate of  $250\text{ mV s}^{-1}$ ) [39, 40]. Each electrode was then analyzed with electrochemical impedance spectroscopy (EIS) to ensure appropriate electrode surface properties and EC behavior ( $37^\circ\text{C}$   $1 \times$  phosphate buffered saline (PBS),  $10\text{ mV}_{\text{rms}}$ ,  $1\text{--}100\text{ 000 Hz}$ ).

**2.3.2. Insertion testing.** Parylene’s flexibility is an advantage for reducing mechanical mismatch with tissue, but it is challenging to insert the probe into cortical tissue. Insertion shuttles or other methods to temporarily provide the required stiffness to insert the probe into cortical tissue have been explored but typically for single probes [25, 37, 41, 42]. We developed a new insertion shuttle to precisely position all four

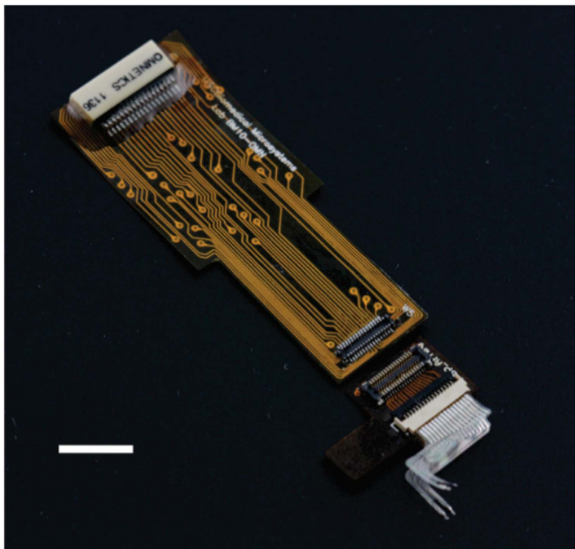


**Figure 5.** The fully packaged  $2 \times 2$  PSEA connects to an adapter with a BM10 connector to interface with the data acquisition system through an Omnetics connector. Scale bar = 1 cm.

probes of the PSEA into cortical tissue simultaneously, building upon our previous insertion shuttle for placing two probes at once [37]. Two pairs of blunt-tipped tungsten microwires ( $300 \mu\text{m}$  diameter, MicroProbes for Life Sciences, Gaithersburg, MD) were affixed side-by-side onto laser-engraved grooves on an acrylic shuttle with superglue and positioned to create a  $2 \times 2$  array spanning a  $1 \text{ mm} \times 1 \text{ mm}$  square to target the rat M1 motor cortex. This ensured proper spacing of the four sheaths as each sheath on the  $1 \times 2$  arrays was affixed to one of these microwires prior to insertion. An additional microwire ( $150 \mu\text{m}$  diameter) served as a fiduciary depth guide during the automated insertion process.

The PSEA was temporarily attached to the insertion shuttle with a small quantity of polyethylene glycol (PEG 3000, Sigma Aldrich, St. Louis, MO), a biodegradable material commonly used for medical applications, in two steps. In the first, the arm of the FPC of the PSEA was attached to the acrylic shuttle using molten PEG 3000 and was aligned so that the four sheaths were in line with the microwires. Following attachment of the FPC of the PSEA on the shuttle, the sheaths were mounted onto the microwires using molten PEG 3000 such that the microwires were positioned directly behind the sheaths. This is in contrast to our earlier approach in which sharp microwires were adhered with PEG to the backside of probes [37]. The stiffness of the thermoformed sheaths was leveraged to penetrate the tissue with the microwires serving as pushrods. In this way, the penetration profile of the insertion shuttle, and thus trauma to the neural tissue, was minimized. The sheaths were attached two at a time so that one  $1 \times 2$  array would be affixed first, and then the tool would be flipped over and the  $1 \times 2$  array on the backside of the FPC would be attached to complete a  $2 \times 2$  orientation of the sheaths (figure 6).

Insertion testing of the PSEA was conducted in a brain phantom model of 0.5% agarose (A9539-50G; Sigma-Aldrich, St. Louis, MO), which closely imitates the

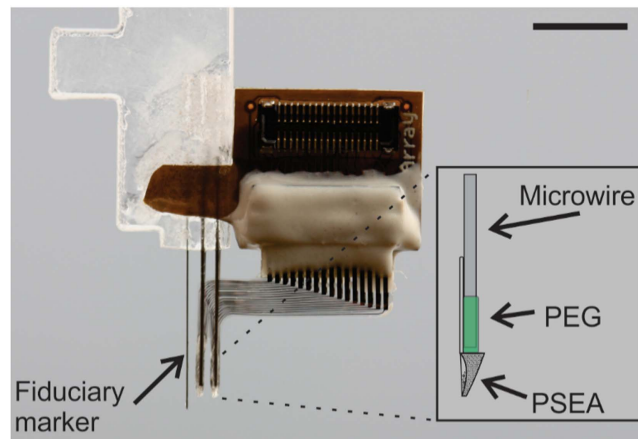


**Figure 6.** Image of a  $2 \times 2$  PSEA temporarily affixed to the insertion shuttle. The inset shows a schematic depicting how each sheath of the PSEA is attached to a tungsten microwire pushrod using PEG 3000. Scale bar = 5 mm.

mechanical properties of cortical tissue [43, 44]. Once the insertion shuttle and PSEA were positioned with the fiduciary depth guide, a linear motor (Thor Labs, Inc., Newton, NJ) inserted the PSEA at a speed of  $0.8 \text{ mm s}^{-1}$ . PBS was then applied to aid in dissolution of the PEG. After 5 min, the shuttle was withdrawn leaving the PSEA in the brain phantom.

#### 2.4. Bioactive interventions

**2.4.1. Coating of the PSEA with bioactive molecules.** To coat the PSEA, a cocktail of bioactive molecules was combined to improve the chronic signal-to-noise ratio and increase the lifetime of the implant. Matrigel (MG) (BD Biosciences, San Jose, CA) was chosen as a basement matrix as it supports neuronal growth, attachment, and differentiation [45, 46]. This matrix was then loaded with two different growth factors to further promote neuronal growth and differentiation and one immunosuppressant to mitigate the brain's immune response. Nerve growth factor (NGF) and brain derived growth factor (BDNF) have been shown to support neuronal growth and have been incorporated into neural probes to guide neurons to electrodes [47–50]. Dexamethasone (DEX) is an anti-inflammatory and immunosuppressant glucocorticoid steroid developed in the late 1950s [51, 52] that has been incorporated into neural probe implantations to reduce the immune response of the cortex [13, 53–57]. In this study, the coating consisted of a 3:1 ratio by volume of MG to PBS. The coating contained  $1 \mu\text{g ml}^{-1}$  of NGF,  $10 \mu\text{g ml}^{-1}$  of BDNF, and  $1.6 \text{ mg ml}^{-1}$  of DEX. To isolate the influences of the MG alone and the additional factors, devices were implanted either with no coating (control), with only the MG coating (Matrigel), or with the MG coating loaded with NGF, BDNF, and DEX (Matrigel+).

The hydrophobic nature of Parylene hinders the application of these water-soluble bioactive molecules. Several methods were investigated to facilitate the application of bioactive coatings and the most effective technique involved the use of poly-D-lysine (P6407, Sigma Aldrich, St. Louis,

MO) to alter the surface energy of the Parylene, making it more hydrophilic to allow for coating with bioactive molecules. To apply the poly-D-lysine, the PSEA was first briefly immersed into 70% ethanol and then into a 100  $\mu\text{l ml}^{-1}$  solution of poly-D-lysine for 1 h at 4 °C. The PSEA was then rinsed with triple distilled water and dried at room temperature. To apply the coating mixture, the poly-D-lysine-coated PSEA was incubated in a droplet of the coating mixture at 50 °C for 5 min. The PSEA was then removed from the coating mixture and the coating was dehydrated for an additional 5 min at 50 °C.

**2.4.2. Virally mediated Caveolin-1 expression.** The viral construct for expression of Caveolin-1 was provided by Dr Brian Head at Raft Therapeutics Inc. and the University of California, San Diego. The AAV9-SynCav (Caveolin-1 gene with synapsin promoter, titer  $3 \times 10^{12} \text{ ml}^{-1}$ ) construct was previously shown to improve neuronal survival and growth *in vitro* by enhancing neuronal membrane/lipid raft formation, increasing expression of neurotransmitter receptors, and promoting neuronal arborization [38].

### 2.5. Ethylene oxide sterilization

Prior to implantation, the PSEA was PEG-attached onto an insertion shuttle and the insertion shuttle was then mounted on a custom probe holder (metal shaft with a plastic block at the bottom). The entire assembly was then sterilized with ethylene oxide for 24 h using a room-temperature system (Anprolene AN74i, Andersen Products, Haw River, NC). After sterilization, probes were stored at 4 °C prior to implantation (~1–2 d). The EC effects of the sterilization process was investigated in a separate study and found to be negligible [58]. However, the sterilization process was found to degrade a portion of the factors across all samples (approximately 13%, 37%, and 47% degradation for DEX, BDNF, and NGF, respectively), as observed through enzyme-linked immunosorbent assay (ELISA), likely due to the amount of time spent in a dry environment at room temperature [59].

### 2.6. Procedure for chronic cortical implantation of PSEA and viral injection

All procedures for the animal experiments were in accordance with the animal protocol approved by the Huntington Medical Research Institutes Institutional Animal Care and Use Committee. A total of 20 animals with  $2 \times 2$  PSEAs were implanted, including 6 animals implanted with uncoated PSEAs, 6 animals with Matrigel-coated PSEAs (Matrigel group), 6 animals implanted with PSEAs coated with Matrigel loaded with neurotrophins and an immunosuppressant (Matrigel+ group), and two animals with virally mediated Caveolin-1 expression (Caveolin-1 group) (table 1).

The chronic implantation surgery was performed in the rat M1 motor cortex of young male Sprague Dawley rats (>320 g) as follows. Anesthesia was induced by placing the rat in a chamber filled with 4% isoflurane in 1 Lpm oxygen.

**Table 1.** Sample groups for chronic implantation.

Sample group	Bioactive intervention	Number of animals
Control	Uncoated probe	6
Matrigel	Probe coated with Matrigel	6
Matrigel+	Probe coated with Matrigel loaded with NGF, BDNF, and DEX	6
Caveolin-1	Uncoated probe, animal injected with Caveolin-1	2

The animal was then placed in a stereotaxic frame (Small animal stereotaxis; Kopf Instruments, Tujunga, CA) and 1%–3% isoflurane in 1 Lpm oxygen was administered via a nose cone. Following a 2 cm long midline incision and retraction of the skin, six holes were drilled into the skull to allow for attachment of a titanium headplate (used as reference/ground) with six stainless steel screws. A craniotomy was made centered at +1.5 mm AP and 1.5 mm ML from bregma, exposing the M1 cortex. The dural membrane over the target area was incised and retracted. The PSEA/insertion shuttle assembly mounted on the probe holder was positioned over the opening area using a stereotaxic apparatus and with the help of the fiduciary depth guide protruding from the insertion shuttle. The assembly was then inserted through the pia and 2 mm into the cortex with a motorized drive (microsyringe pump UltraMicroPump UMP3, WPI) at a speed of 0.8 mm s<sup>-1</sup>. Following insertion, bone cement was applied to the skull below the lateral portion of the PSEA to anchor the PSEA in place. After allowing five minutes for the bone cement to cure, saline was applied to allow for PEG dissolution and separation of the PSEA from the insertion shuttle, and the shuttle was withdrawn. Gelfoam was applied to cover the craniotomy and additional bone cement was applied over Gelfoam and surrounding skull to create the head cap around the PSEA and connector, securing the FPC to the headplate and skull. The skin was then sutured around the head cap (4-0 nylon monofilament sutures; Keebomed Inc., Morton Grove, IL). The animal was kept on a warming pad in a recovery cage until it was fully awake and sternal, at which point the animal was returned to its housing cage.

In the Caveolin-1 group, we performed microinjections of the viral construct, AAV9-SynCav1, in the M1 cortex. Microinjections were done at 9 cortical sites spaced 0.5 mm apart rostro-caudally and medio-laterally with a 35-gauge needle (OD 135  $\mu\text{m}$ ) mounted on a 10  $\mu\text{l}$  microsyringe pump (UltraMicroPump UMP3, WPI) inserted to a depth of 1.7 mm using a three-dimensional precision micromanipulator. At each cortical site, a 1  $\mu\text{l}$  volume of AAV9-SynCav1 was slowly injected at a speed of 0.5  $\mu\text{l min}^{-1}$ ; the needle was left in place for additional 2 min before retraction to prevent backflow. The PSEA was then inserted into the same cortical area immediately following the viral injections.

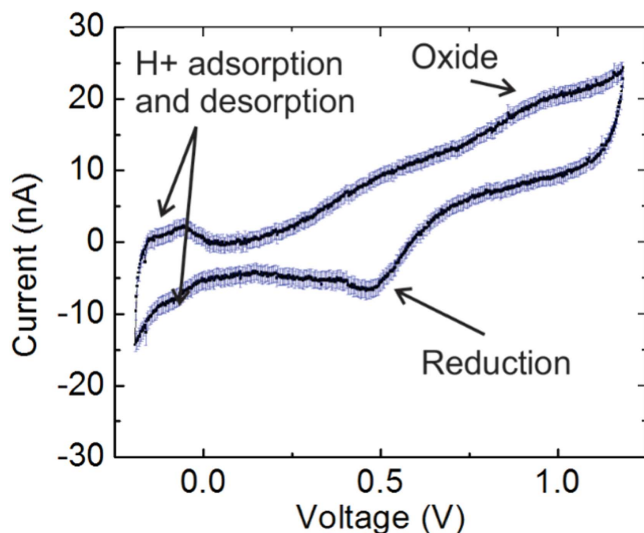


**Figure 7.** CV of the PSEA in 0.05 M  $\text{H}_2\text{SO}_4$  showing expected redox peaks. Mean  $\pm$  SE,  $n = 703$  electrodes across 89 sheaths.

### 3. *In vivo* testing

To assess the functionality of PSEA, *in vivo* EIS and neural recordings were carried out weekly (starting at week 1) or biweekly (starting on week 30) and ending at or shortly before animal's sacrifice time (week 14–52 post-implantation). During testing, the rats were anesthetized with ketamine/xylazine ( $90/10 \text{ mg kg}^{-1}$ , IP).

#### 3.1. EIS recordings

*In vivo* EIS measurements were obtained using a PC4/300 potentiostat system (Gamry Instruments, Warminster, PA) in a two-electrode configuration, with the reference and counter connected to the titanium headplate. The data were collected with  $10 \text{ mV}_{\text{rms}}$  sinusoids at frequencies from 1 Hz to 100 kHz. The impedance values at 1 kHz were selected for analysis due to the correspondence of this frequency to the bandwidth of neural signals in the brain.

#### 3.2. Electrophysiology recordings

Electrophysiological data were acquired at 16 bit and 40 kHz per channel using a 64-channel data acquisition system (OmniPlex; Plexon Inc., Dallas, TX) and high-pass filtered at 300 Hz to remove the low-frequency fluctuations from the baseline.

#### 3.3. Spike detection, determination of SNR

The collected data were used to calculate three performance metrics: *unresolved neural noise*, *signal-to-noise ratio (SNR)*, and *firing rate*. In the 120 s (sec) data records, spike detection was performed using the nonlinear energy operator (NEO) method, which allows more accurate spike detection at low SNRs as compared to a more commonly used amplitude thresholding method [60]. The neuronal noise was calculated as the standard deviation of the data after removal of 0.8 ms-

long segments containing the detected spikes. The spike amplitude was calculated as the absolute value of spike's peak height. The average spike amplitude for the record was calculated using all detected spikes. Spike sorting was not applied to remove false positives, as the data was collected while the rats, along with the connected headstage and pre-amplifier, were placed in a Faradaic cage, eliminating externally generated electromagnetic interference at the Hz–kHz frequency range. Furthermore, there were no electromyographic artifacts, as the ketamine/xylazine anesthesia was sufficiently deep to suppress animal movements. Since both the average spike amplitude and average noise were calculated as monophasic values (as opposed to the biphasic peak-to-peak amplitude calculation), the SNR was calculated simply as the ratio of these values. The firing rate was also calculated for all spike-like events. The SNR and firing rate values were calculated for a record only if 10 or more spike-like events were detected in 120 s.

#### 3.4. Histology

Within an hour after the last electrophysiological test, the rats were injected with heparin sulfate ( $1000 \text{ IU/kg}$ , IP), while still anesthetized with ketamine/xylazine ( $90/10 \text{ mg kg}^{-1}$ , IP), and transcardially perfused with 100 ml of a pre-wash containing PBS with heparin ( $5 \text{ IU ml}^{-1}$ ) followed by 200 ml of phosphate buffered 4% paraformaldehyde solution. The head was removed and immersion-fixed in 4% paraformaldehyde overnight. The next day, cerebral cortex dissection was performed. An effort was made to keep the probe inside the cortex during the removal of the bone cement-encapsulated PSEA. In several cases, however, the probe came out from the cortex due to insufficient connective tissue encapsulation to hold it in place. The cortical tissue block containing the probe tracks (and the probes, if still in place) was embedded into paraffin. The tissue was sectioned at a thickness of  $10 \mu\text{m}$  in a direction perpendicular to the probe tracks. The sections were then double-immunostained for GFAP (marker for reactive astrocytic processes) and for NeuN (neuronal marker). The primary antibodies were anti-NeuN (MAB377, 1:2000, Chemicon, Temecula, CA) and anti-GFAP (Z0334, 1:10 000, Dako Corp., Carpinteria, CA), and the chromogens were Vector nickel-DAB (for NeuN) and Vector Red (for GFAP). Tissue sections were photographed using a color CCD microscope camera (Grasshopper Express 2.8 MP, Point Grey Research).

## 4. Results

### 4.1. *In vitro* characterization

**4.1.1. Electrochemical characterization.** The voltammogram acquired from the EC cleaned electrode sites demonstrated effective cleaning of the surface. The final cycle presents redox peaks for oxide formation and reduction and the

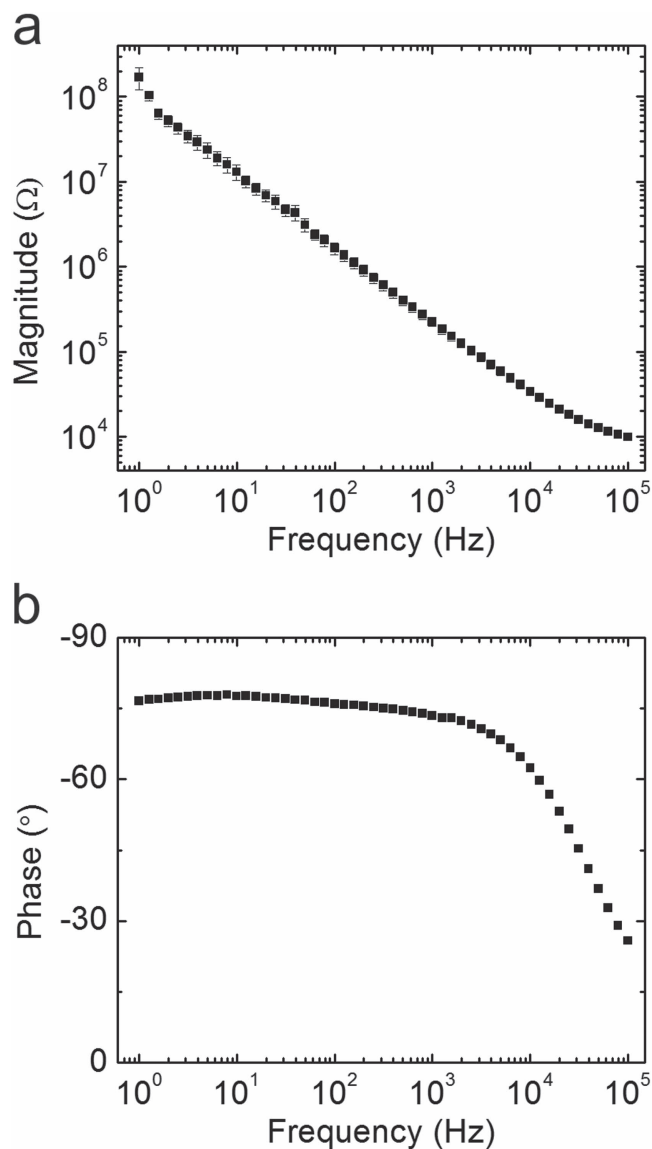


**Figure 8.** Impedance magnitude (a) and phase (b) of the PSEA. Mean  $\pm$  SE,  $n = 715$  electrodes across 94 sheaths.

adsorption/desorption of hydrogen, which is expected for a platinum electrode surface in  $\text{H}_2\text{SO}_4$  (figure 7).

Following EC cleaning, EIS measurements indicated consistent performance across devices with very little variability amongst devices from the same wafer as well as between wafers, as seen in figure 8. It was previously determined that the coating process changed the EIS of an uncoated probe with a slight increase in impedance [59]. Due to the water-soluble nature of the coatings, EIS of each PSEA electrode was conducted only prior to coating. At 1 kHz, average electrode impedance was found to be  $226.7 \pm 28.4 \text{ k}\Omega$  (mean  $\pm$  SE,  $n = 715$  electrodes across 94 sheaths), which is appropriate for intracortical recording applications [61].

**4.1.2. Insertion testing.** Insertion testing conducted in agarose showed successful insertion of the PSEA sheaths. However, it was previously observed that the sheaths

retracted  $86.3 \pm 36.0 \mu\text{m}$  (mean  $\pm$  SD,  $n = 6$  trials) when the shuttle was withdrawn [37]. This was attributed to surface tension between the microwires on the insertion shuttle and the PSEA from the saline and dissolved PEG. To compensate, a deeper insertion was required so that the expected retraction *in vivo* resulted in placement of the PSEA in the desired location.

#### 4.2. *In vivo* study

**4.2.1. Implantation.** In comparison with our initial one-month study [37], we made several improvements to the implantation technique. First, we adopted the pushrod insertion shuttle, which was simple to use and produced less displacement of cortical tissue during the insertion than our earlier methods. Minimizing displacement was essential given the small target volume and the increased number of probes (from 2 to 4). Second, we used a motorized drive, which improved the consistency of speed and depth penetration, which was important given the quick dissolution of PEG in the tissue. Third, the craniotomy was covered with Gelfoam instead of Kwik-Sil silicone for protecting the cortex from bone cement. Kwik-Sil adheres to both the probe and the overlying bone cement, thus the probes often pulled out while removing the cemented headcap. In addition, Gelfoam (unlike the Kwik-Sil) degrades soon after implantation and is replaced with a layer of loosely organized connective tissue, which provides strain relief between the probes and the cable and provides the access to the PSEA cable during the dissection for separating the probes from the rest of the assembly and headcap. Just as in our initial one-month study, a titanium headplate was screwed into the skull surrounding the craniotomy and the FPC was affixed to the skull and secured head plate with bone cement, keeping the BM10 connector exposed for connection, as seen in the last frame of figure 9.

**4.2.2. EIS and electrophysiology.** Neural recordings were collected weekly (in a few animals surviving beyond week 30, the recordings were then done biweekly) and the spikes were detected using the NEO thresholding method, as described in the methods. Detected spikes from a representative electrode in a long-surviving animal from the Caveolin-1 group are shown in figure 10.

Comparison of electrochemical and electrophysiological performance at 10–14 weeks (figure 11) indicated that the control uncoated group had a significantly lower electrochemical impedance and smaller SNR compared to the other groups. This suggests that Matrigel-containing coatings and virally mediated Caveolin-1 expression had a beneficial effect on probe integration with the tissue and on the electrophysiological performance. The best electrophysiological performance, in terms of firing rate and SNR, was exhibited by the Matrigel+ and Caveolin-1 groups. Although the electrode impedance, noise level, and SNR were comparable between the Matrigel and Matrigel+ groups, the increased firing rate observed in the Matrigel+ group indicates that the included NGF, BDNF, and DEX had a positive impact on

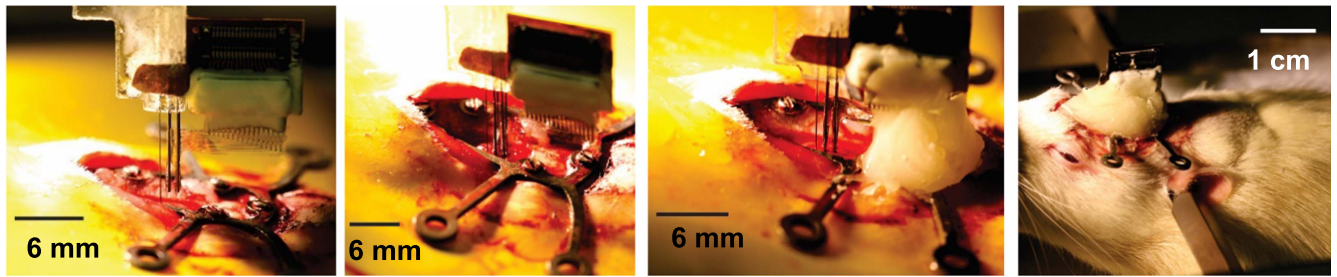


**Figure 9.** Implantation steps. From left to right: initial contact with the pia, immediately after the insertion, after first application of bone cement, and after placing Gelfoam and second application of bone cement.

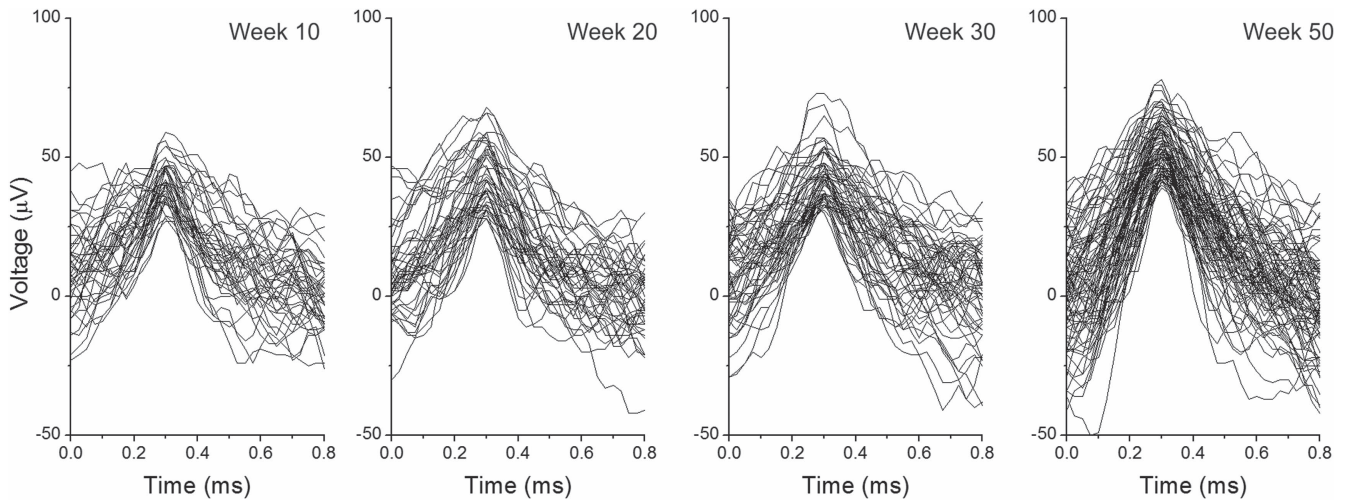


**Figure 10.** Spikes detected by the NEO method at 40 s-long neural recordings from a representative electrode in PSEA probe #1 implanted in the animal from the Caveolin-1 group. The recordings were collected at 10, 20, 30, and 50 weeks after implantation, as indicated in the labels.

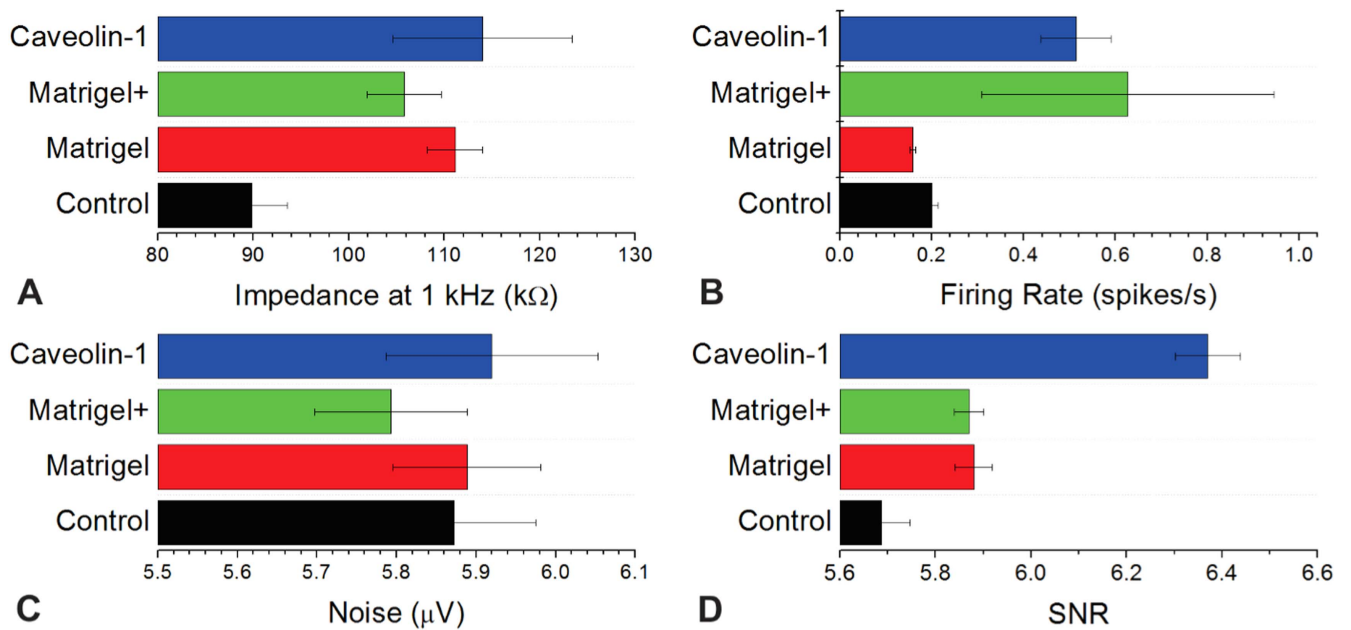


**Figure 11.** Levels of (A) 1 kHz impedance, (B) firing rate, (C) noise, and (D) SNR at 10–14 weeks post-implantation for four coating groups. Error bars indicate the standard error.

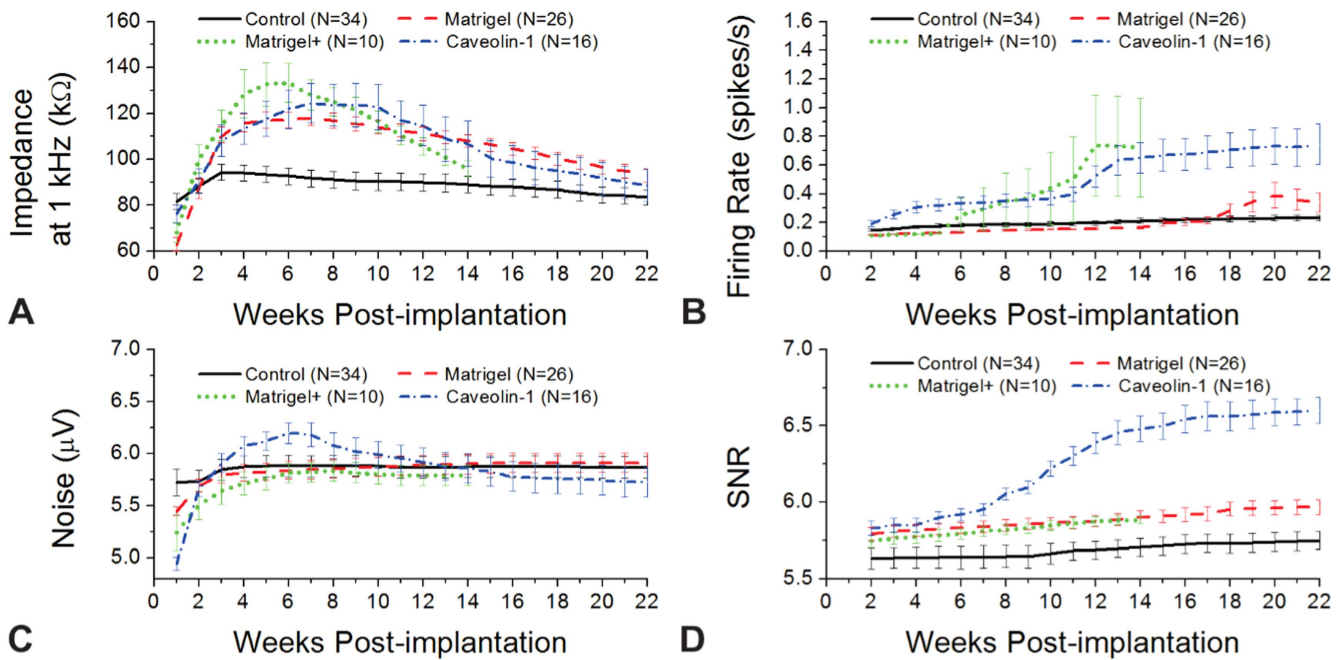


**Figure 12.** Changes in (A) 1 kHz impedance, (B) firing rate, (C) noise, and (D) SNR over time after the PSEA implantation for four coating groups. Values in the legend (in parentheses) indicate the number of chronically functional electrode sites per group. Error bars indicate the standard error.

neuronal activity despite any degradation that may have occurred during the sterilization process.

Temporal dynamics of the electrochemical and electrophysiological performance were evaluated for the 22-week-long post-implantation period, as the animals from multiple groups were sacrificed at that time point (animals in the Matrigel+ group were sacrificed earlier at 14 weeks) (figure 12). Temporal dynamics of 1 kHz impedance measurements indicated their initial rise and delayed decrease (figure 12(a)). The initial rise was likely caused by the electrode encapsulation, while the delayed decrease could have been caused either by a degradation of the PSEA probe insulation or by a chronic glial response at the electrode-tissue interface. The noise level increased in the first 4–6 weeks and then remained relatively constant in all groups (figure 12(c)). Resolvable multiunit neural activity was not detected (and, therefore, SNR was not calculated) during week 1, first appeared at week 2 and then gradually increased over the course of 12–14 weeks and reached a plateau of performance (figures 12(b) and (d)).

Detailed examination of electrophysiological performance in two long-surviving animals—first from the Caveolin-1 group (figure 13) and second from the Matrigel group (figure 14)—demonstrated considerable variability among four probes implanted side-by-side over the 52-week post-implantation period. The best performing 8-electrode PSEA probe (#1) in the Caveolin-1 animal exhibited a remarkable gradual improvement in the firing rate despite the stable levels of impedance, noise, and SNR, suggesting plastic changes in the neuronal activity levels, perhaps indicative of a continued virally mediated Caveolin-1 expression in the cells (figure 13). In the animal from the Matrigel group, the noise level in probe #1 was considerably

higher, while the firing rate and SNR performance were similar in probes #1 and #2 (figure 14).

#### 4.3. Immunohistochemistry

Immunohistochemical evaluation was performed on the cortical tissue from two long-surviving animals—first from the Caveolin-1 group (figure 15) and second from the Matrigel group (figure 16)—in order to examine whether the local tissue environment surrounding the probes contributed to their variable electrophysiological performance within the same PSEA (figures 13 and 14). As can be seen in both animals, there was significant variability in the density of NeuN-stained neurons and GFAP-positive reactive astrocytosis in the cortical tissue around each of four probes.

In the Caveolin-1 animal (figure 15), probes #1 and #2 exhibited a closer apposition of neurons to the probe's surface and lower density of reactive astrocytosis (as compared to probes #3 and #4), which correlates with the detection of resolvable neural activity by these probes (figure 13). In the same animal, NeuN staining was also apparent inside the probe #1, which correlates with a higher SNR and firing rate in that probe as compared to probe #2, suggesting sprouting of dendrites through the perforations.

In the Matrigel animal (figure 16), probes #1 and #2 also exhibited a closer apposition of neurons to the probe's surface and lower density of reactive astrocytosis (as compared to probes #3 and #4), which correlates with the detection of resolvable neural activity by these probes (figure 14). No NeuN staining was apparent inside these probes (with a caveat that some of the tissue inside the lumen was detached during the slide staining process), correlating

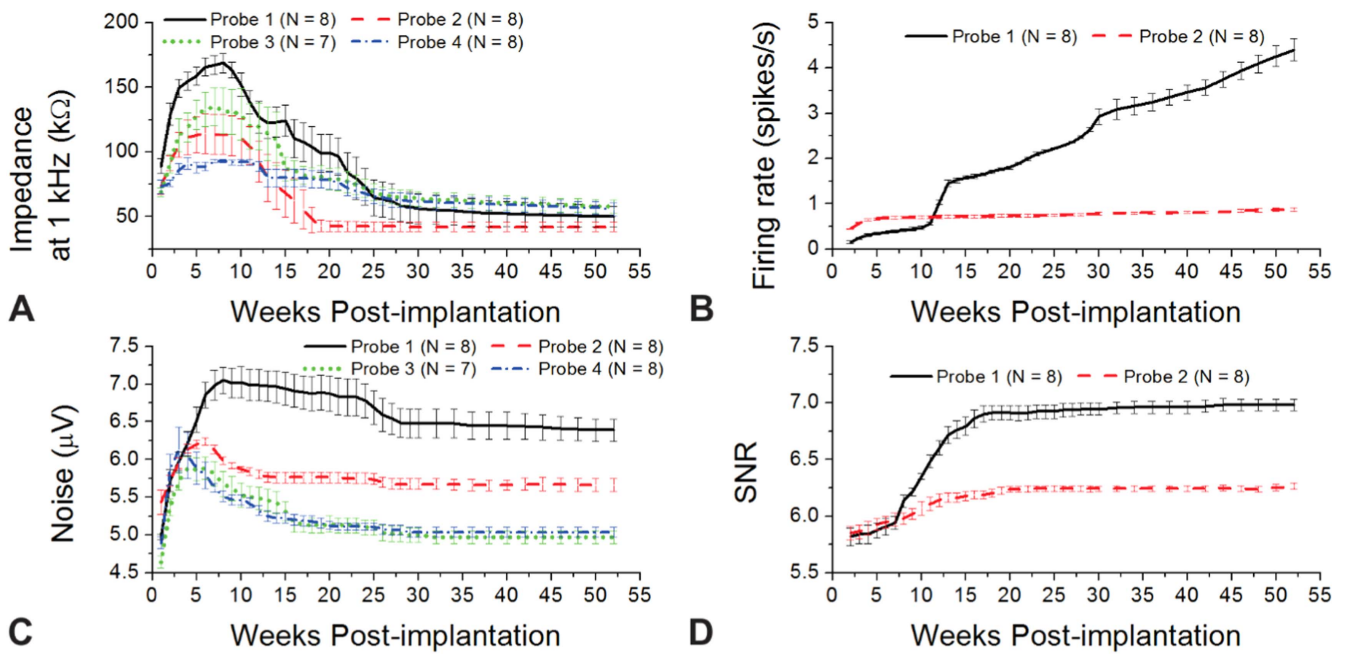


**Figure 13.** Changes in (A) 1 kHz impedance, (B) firing rate, (C) noise, and (D) SNR over time after the PSEA implantation for four probes (labeled 1 through 4) in the animal from Caveolin-1 group. Probes 3 and 4 are not shown in (B) and (D) due to a lack of resolvable neural activity. Values are the averages of all functional electrodes per probe, as indicated in parentheses. Error bars indicate the standard error.

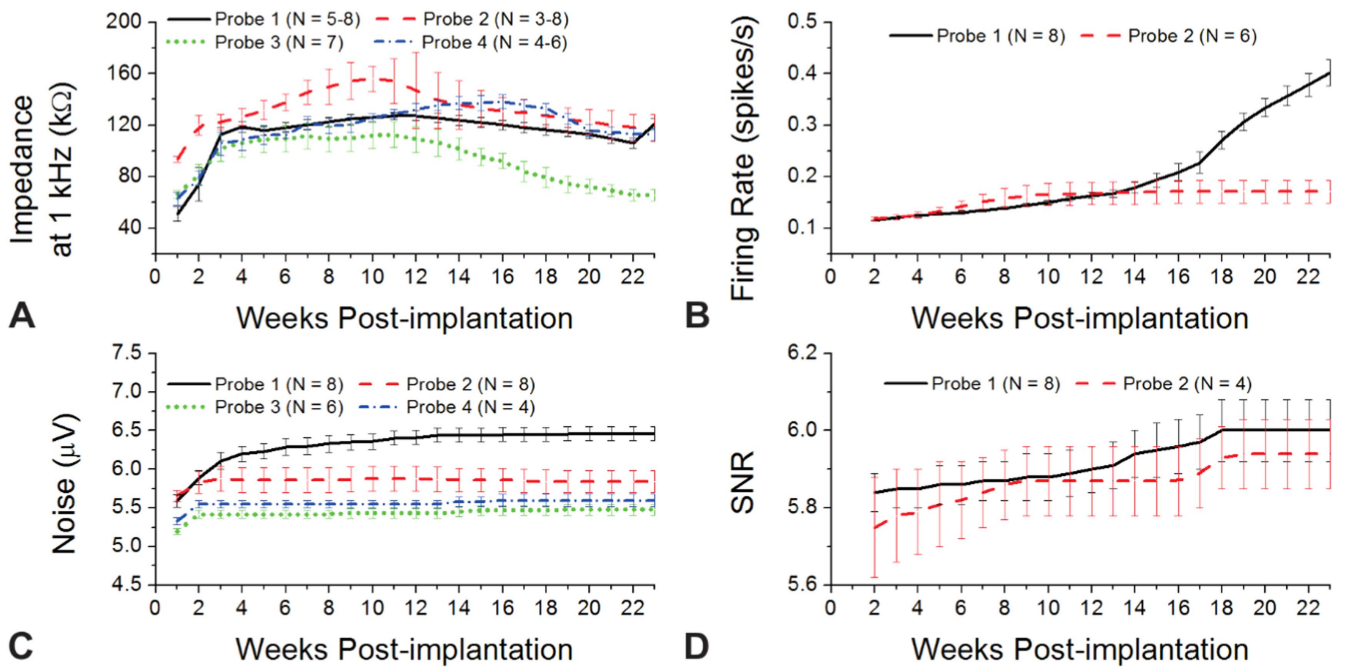


**Figure 14.** Changes in (A) 1 kHz impedance, (B) firing rate, (C) noise, and (D) SNR over time after the PSEA implantation for four probes (labeled 1 through 4) in the animal from Matrigel group. Probes 3 and 4 are not shown in (B) and (D) due to a lack of resolvable neural activity. Values are the averages of all functional electrodes per probe, as indicated in parentheses. Error bars indicate the standard error.

with their low SNRs and firing rates (as compared to the probe #1 in the Caveolin-1 animal).

Finally, we have compared the changes in neural signals (i.e. amplitudes of resolvable action potentials) at 3 weeks versus the last pre-sacrifice time point, and observed similar increases in the signals in both long-surviving animals (figure 17). In both the Matrigel and the Caveolin-1 animal, there was a slight, but statistically insignificant, signal

increase for the electrode sites located inside the probe sheath as compared to those outside the sheath. This is in sharp contrast with our previous study in which, at 28 weeks, a higher SNR was observed from the outer rather than the inner electrodes of Matrigel-coated probes [37].

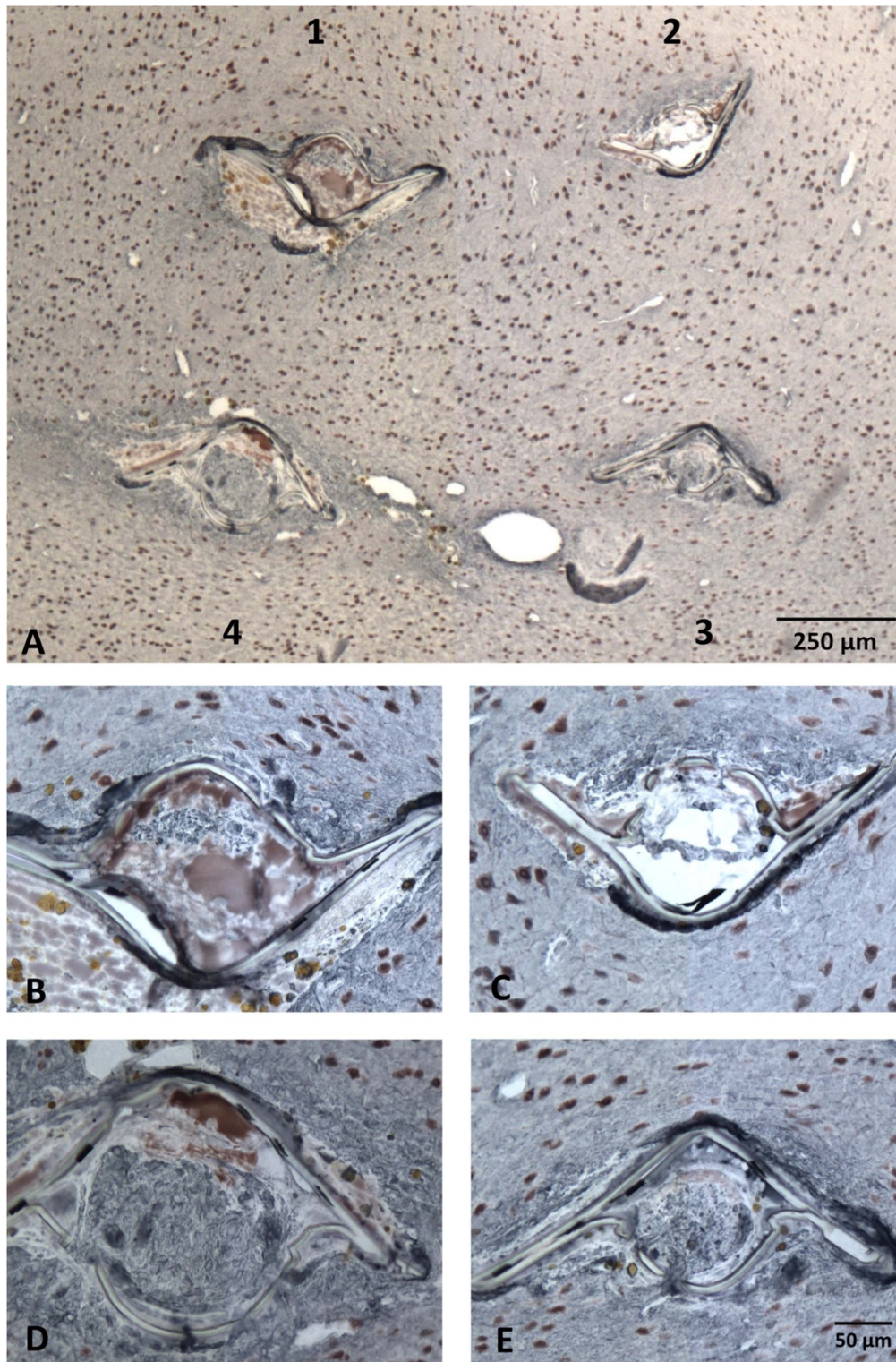


**Figure 15.** Microphotographs of the cerebral cortex cut perpendicular to four probes in the animal from Caveolin-1 group double-stained with antibodies for NeuN (brown) and GFAP (dark-blue). (A) Overview of four probes labeled 1 through 4. (B)–(E) Close-up views of individual probes showing variable NeuN staining adjacent and inside the probe and variable GFAP staining around the probe.

## 5. Discussion

A 3D Parylene intracortical neural probe array was designed, fabricated, characterized, and successfully implanted into the rat motor cortex for 12 months. 32 electrodes distributed

across four 3D sheath structures allowed for a higher electrode count and density to interface with more neurons and improved recording quality than with the  $1 \times 2$  array design utilized in our previous one-month study. Moreover, this design is highly scalable with minimal modifications as

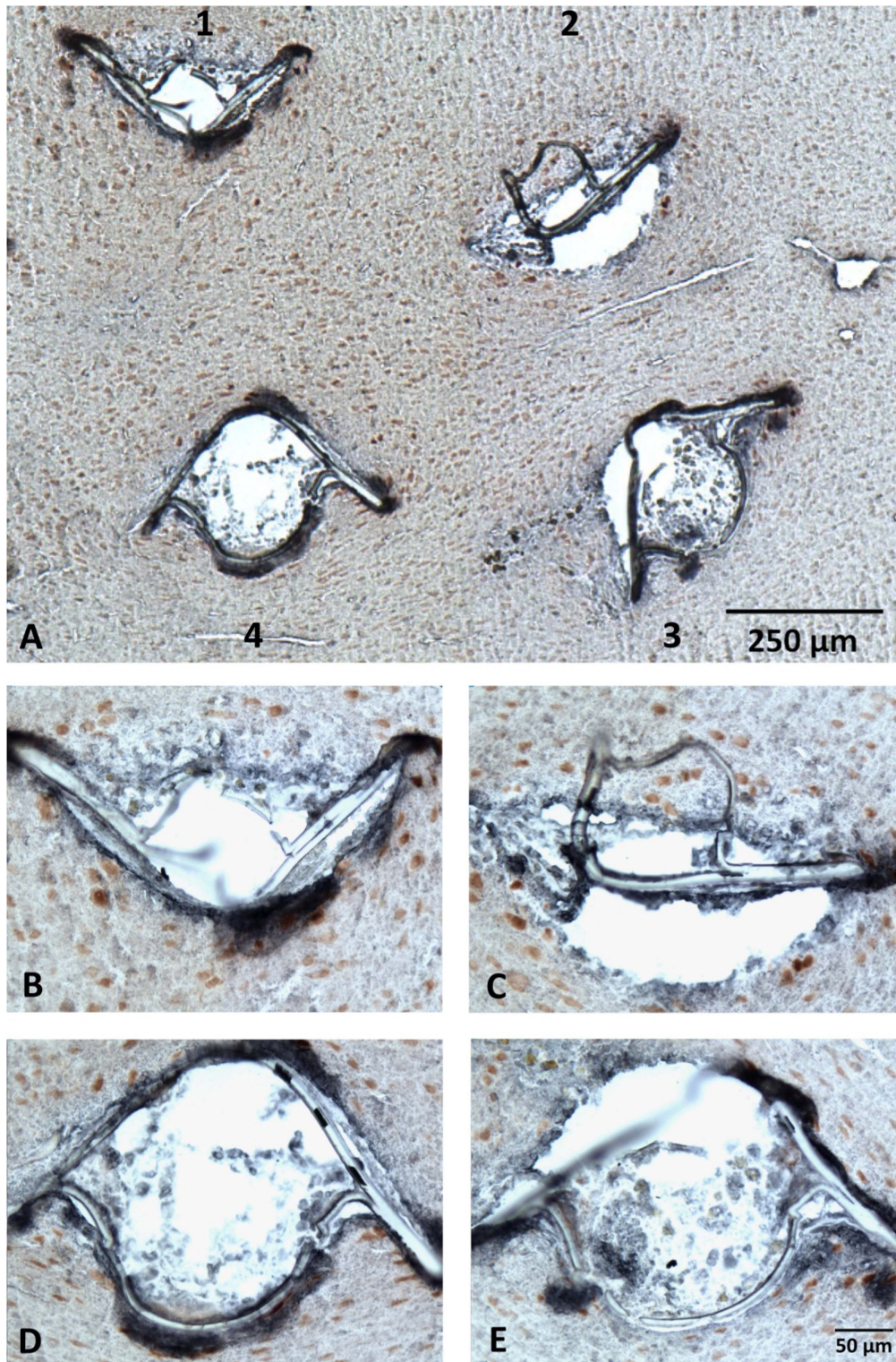


**Figure 16.** Microphotographs of the cerebral cortex cut perpendicular to four probes in the animal from Matrigel group double-stained with antibodies for NeuN (brown) and GFAP (dark-blue). (A) Overview of four probes labeled 1 through 4. (B)–(E) Close-up views of individual probes showing variable NeuN staining adjacent and inside the probe and variable GFAP staining around the probe.

multiple arrays containing any number of probes each can be combined on an FPC in a similar fashion as demonstrated here. For example, the  $1 \times 2$  arrays can easily be made into  $1 \times 4$  or  $1 \times 8$  arrays by adjusting the layout. These can then be stacked using the technique developed here into  $4 \times 4$  or

$8 \times 8$  arrays. The only practical limitation is the available channel count in commercially available ZIF connectors. Microfabricated entirely from Parylene and platinum materials, the PSEA utilized the flexibility of Parylene to minimize inflammatory response in the surrounding tissue. The sheath

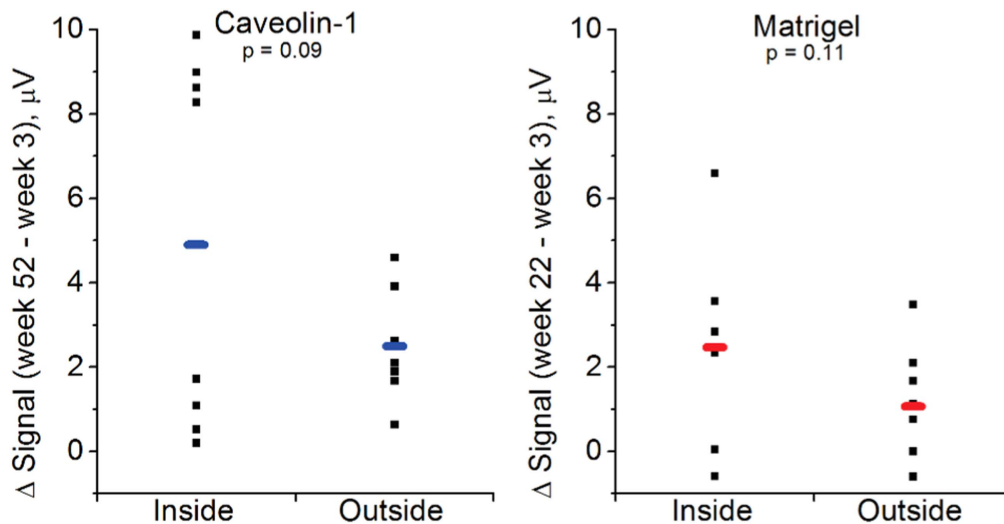


**Figure 17.** Changes in the neural signal level (i.e. average amplitude of resolved action potentials) between the latest pre-sacrifice time point and week 3 for two long-surviving animals: first from the Caveolin-1 group (left) and second from the Matrigel group (right). Scatter plots show the values from individual electrode sites located inside and outside of the probe sheath. Horizontal bars are the averages of 6–8 electrode sites from probes #1 and #2, where resolvable neural activity was detected.

structures featured a sharp taper in order to reduce damage to tissue during insertion, based on the taper optimization performed in the previous study [37]. Additionally, perforations were placed throughout the sheath to improve chemical signaling between cells and to promote dendritic sprouting. The EC properties of the electrodes were evaluated *in vitro* and found to be appropriate for neuronal recording. Additionally, very little variability was observed over 766 electrodes from 96 different sheath structures, indicating a very consistent fabrication and electrode cleaning process. Prior to implantation, the PSEA was coated with Matrigel loaded with NGF, BDNF, and DEX to encourage neural integration and to suppress the immune response. The hydrophobic nature of Parylene was concealed through the use of poly-D-lysine, which uniformly coated all PSEA surfaces, including the sheath interior. A custom insertion shuttle was developed to temporarily provide the necessary stiffness for inserting the PSEA into cortical tissue and then to retract, leaving only the compliant PSEA in the tissue.

Longitudinal electrophysiological measurements revealed improved SNR at probes with bioactive interventions as compared with the control. Although the Matrigel coating exhibited a higher SNR than the uncoated control, it exhibited very similar firing rates. However, the inclusion of NGF, BDNF, and DEX into the Matrigel coating (Matrigel+) was shown to improve neuronal firing rate over the use of a Matrigel coating alone, suggesting that they provide additional support to neuronal health. These results and previous work which has shown that these factors elute from the coating within a short time course [59] suggest that an even greater impact may be achieved through the use of a prolonged release profile or repeated application. However, novel delivery mechanisms would have to be developed and additional studies conducted to investigate that possibility. In the current study, the best performance was observed in probes at which virally mediated Caveolin-1 was expressed, indicating

a superior biological environment for probe integration into tissue.

Immunohistochemical analysis of cortical tissue indicated significant variability in the density of NeuN-stained neurons and GFAP-positive reactive astrocytosis around individual probes, even on a single array within the same animal. Closer apposition of neurons to the PSEA surface (probes #1 and #2 versus probes #3 and #4 in the Caveolin-1 and Matrigel animals) was correlated with the ability to detect resolvable neural activity by these probes. Furthermore, presence of NeuN staining inside the probe #1 in the Caveolin-1 animal was correlated with the highest SNR and firing rate for the electrode sites in that probe (as compared to other probes in that animal and other animals in the study), suggesting that a virally mediated long-term expression of Caveolin-1 may have contributed to dendritic sprouting and was manifested as a gradual increase in the SNR during the first 15 weeks post-implantation and even more protracted rise in the firing rate. To our knowledge, this represents the first example in the literature of a direct correlation between the gradual rise in the neural signaling and histologically observable dendritic sprouting. An alternative explanation for the rise in SNR would be due to deterioration in the Parylene coating of the PSEA, but that explanation is unlikely given the stability of electrical impedance and noise level during that period.

As compared to our earlier one-month study with manually inserted PSEAs [37], in this study we observed less GFAP-positive reactive astrocytosis around the probes. The reduced level of astrocytosis can be attributed to a smaller tissue displacement exhibited by the pushrod insertion shuttle, as compared to the earlier insertion shuttle designs, and the inclusion of perforations throughout the probe structure that enabled cell-to-cell chemical signaling. In contrast with our one-month study, we demonstrated a comparable or slightly greater increase over time for the amplitude of neural signals

for the inner electrode sites as compared to the outer ones in the Matrigel and Caveolin-1 groups. We speculate that Caveolin-1-mediated neurotropic signaling and the supportive biological environment created by Matrigel in combination with the probe perforations and the acellular tissue structure inside the probe sheath provided an attractive environment for dendritic sprouting through perforations into the sheath. In comparison, dendritic sprouting outside the probe was possibly constrained by a presence of a dense astrocytic layer around the probes. Further studies are needed to explore this possibility.

Overall, this study provided support for the importance of creating a supportive biological environment around neural probes to promote stable long-term electrophysiological performance of flexible probes in the cerebral cortex. In particular, we demonstrated the beneficial effects of a Matrigel coating, the inclusion of additional neurotrophins and immunosuppressants into that coating, and the long-term expression of Caveolin-1. Furthermore, we provided support to the idea of using an artificial acellular tissue compartment as a way to counteract the walling-off effect of the astrocytic scar formation around the probes as a means of establishing a more intimate and stable neural interface.

## Acknowledgments

This work was sponsored by the Defense Advanced Research Projects Agency (DARPA) MTO under the auspices of Dr Jack Judy through the Space and Naval Warfare Systems Center, Pacific grant/contract no. N66001-11-1-4207. The authors would also like to thank the following individuals at the Huntington Medical Research Institutes: Dr Douglas McCreery for advice on probe development and insertion shuttle design and for helpful comments on the manuscript, Dr Martin Han for providing the electrophysiological recording system and for assistance in analysis of some of the electrochemical data, Dr Saiyun Hou for performing the chronic animal implantations and transcatheter perfusions, Ms. Nijole Kuleviciute for collection of *in vivo* impedance spectroscopy data, Mr Jesus Chavez for immunohistochemical staining, and Mr Haison Duong for image capturing. We thank Dr Brian Head at Raft Therapeutics Inc. and the University of California, San Diego for the AAV9-SynCav1 viral construct. We also thank Dr Donghai Zhu of the Keck Photonics Laboratory for help with fabrication, and members of the Biomedical Microsystems Laboratory of USC for their assistance.

## References

- [1] Polikov V S, Tresco P A and Reichert W M 2005 Response of brain tissue to chronically implanted neural electrodes *J. Neurosci. Methods* **148** 1–18
- [2] He W and Bellamkonda R V 2008 A molecular perspective on understanding and modulating the performance of chronic central nervous system (CNS) recording electrodes

- Indwelling Neural Implants: Strategies for Contending with the In Vivo Environment* ed W M Reichert (Boca Raton, FL)
- [3] Kozai T D Y 2015 Brain tissue responses to neural implants impact signal sensitivity and intervention strategies *ACS Chem. Neurosci.* **6** 48–67
  - [4] Saxena T, Karumbaiah L, Gaupp E A, Patkar R, Patil K, Betancur M, Stanley G B and Bellamkonda R V 2013 The impact of chronic blood-brain barrier breach on intracortical electrode function *Biomaterials* **34** 4703–13
  - [5] Karumbaiah L, Saxena T, Carlson D, Patil K, Patkar R, Gaupp E A, Betancur M, Stanley G B, Carin L and Bellamkonda R V 2013 Relationship between intracortical electrode design and chronic recording function *Biomaterials* **34** 8061–74
  - [6] Kolarcik C L, Bourbeau D, Azemi E, Rost E, Zhang L, Lagenaur C F, Weber D J and Cui X T 2012 *In vivo* effects of L1 coating on inflammation and neuronal health at the electrode-tissue interface in rat spinal cord and dorsal root ganglion *Acta Biomaterialia* **8** 3561–75
  - [7] Azemi E, Gobel G T and Cui X T 2010 Seeding neural progenitor cells on silicon-based neural probes *J. Neurosurg.* **113** 673–81
  - [8] Biran R, Noble M D and Tresco P A 2003 Directed nerve outgrowth is enhanced by engineered glial substrates *Exp. Neurol.* **184** 141–52
  - [9] Sawyer A J, Tian W, Saucier-Sawyer J K, Rizk P J, Saltzman W M, Bellamkonda R V and Kyriakides T R 2014 The effect of inflammatory cell-derived MCP-1 loss on neuronal survival during chronic neuroinflammation *Biomaterials* **35** 6698–706
  - [10] Kozai T D, Li X, Bodily L M, Caparosa E M, Zenonos G A, Carlisle D L, Friedlander R M and Cui X T 2014 Effects of caspase-1 knockout on chronic neural recording quality and longevity: insight into cellular and molecular mechanisms of the reactive tissue response *Biomaterials* **35** 9620–34
  - [11] Gutowski S M, Templeman K L, South A B, Gaudling J C, Shoemaker J T, LaPlaca M C, Bellamkonda R V, Lyon L A and Garcia A J 2014 Host response to microgel coatings on neural electrodes implanted in the brain *J. Biomed. Mater. Res. A* **102** 1486–99
  - [12] Luo X, Matranga C, Tan S, Alba N and Cui X T 2011 Carbon nanotube nanoreservoir for controlled release of anti-inflammatory dexamethasone *Biomaterials* **32** 6316–23
  - [13] Zhong Y and Bellamkonda R V 2007 Dexamethasone coated neural probes elicit attenuated inflammatory response and neuronal loss compared to uncoated neural probes *Brain Res.* **1148** 15–27
  - [14] Skousen J L, Merriam M E, Srivannavit O, Perlin G, Wise K D and Tresco P A 2011 Reducing surface area while maintaining implant penetrating profile lowers the brain foreign body response to chronically implanted planar silicon microelectrode arrays *Brain Mach. Interfaces* **194** 167–80
  - [15] Seymour J P and Kipke D R 2007 Neural probe design for reduced tissue encapsulation in CNS *Biomaterials* **28** 3594–607
  - [16] Capadona J R, Tyler D J, Zorman C A, Rowan S J and Weder C 2012 Mechanically adaptive nanocomposites for neural interfacing *MRS Bull.* **37** 581–9
  - [17] Nguyen J K, Park D J, Skousen J L, Hess-Dunning A E, Tyler D J, Rowan S J, Weder C and Capadona J R 2014 Mechanically compliant intracortical implants reduce the neuroinflammatory response *J. Neural Eng.* **11** 056014
  - [18] Subbaroyan J, Martin D C and Kipke D R 2005 A finite-element model of the mechanical effects of implantable microelectrodes in the cerebral cortex *J. Neural Eng.* **2** 103
  - [19] Biran R, Martin D C and Tresco P A 2007 The brain tissue response to implanted silicon microelectrode arrays is

- increased when the device is tethered to the skull *J. Biomed. Mater. Res. A* **82** 169–78
- [20] Gilletti A and Muthuswamy J 2006 Brain micromotion around implants in the rodent somatosensory cortex *J. Neural Eng.* **3** 189–95
- [21] Sridharan A, Rajan S D and Muthuswamy J 2013 Long-term changes in the material properties of brain tissue at the implant-tissue interface *J. Neural Eng.* **10** 16
- [22] Du J, Roukes M L and Masmanidis S C 2009 Dual-side and three-dimensional microelectrode arrays fabricated from ultra-thin silicon substrates *J. Micromech. Microeng.* **19** 075008
- [23] Stieglitz T, Beutel H, Blau C and Meyer J-U 1998 Micromachined devices for interfacing neurons *Proc. SPIE* **3324** 174
- [24] Rousche P J, Pellinen D S, Pivin D P Jr, Williams J C and Vetter R J 2001 Flexible polyimide-based intracortical electrode arrays with bioactive capability *IEEE Trans. Biomed. Eng.* **48** 361–71
- [25] Xiang Z, Yen S-C, Xue N, Sun T, Tsang W M, Zhang S, Liao L-D, Thakor N V and Lee C 2014 Ultra-thin flexible polyimide neural probe embedded in a dissolvable maltose-coated microneedle *J. Micromech. Microeng.* **24** 065015
- [26] Takeuchi S, Ziegler D, Yoshida Y, Mabuchi K and Suzuki T 2005 Parylene flexible neural probes integrated with microfluidic channels *Lab Chip* **5** 519–23
- [27] Gilgunn P J, Khilwani R, Kozai T D Y, Weber D J, Cui X T, Erdos G, Ozdoganlar O B and Fedder G K 2012 An ultra-compliant, scalable neural probe with molded biodissolvable delivery vehicle *IEEE 25th Int. Conf. on Micro Electro Mechanical Systems (MEMS)* pp 56–9
- [28] Kuo J T W, Kim B J, Hara S A, Lee C D, Gutierrez C A, Hoang T Q and Meng E 2013 Novel flexible Parylene neural probe with 3D sheath structure for enhancing tissue integration *Lab Chip* **13** 554–61
- [29] Castagnola V, Descamps E, Lecestre A, Dahan L, Remaud J, Nowak L and Bergaud C 2014 Parylene-based flexible neural probes with PEDOT coated surface for brain stimulation and recording *Biosensors Bioelectron.* (doi:10.1016/j.bios.2014.09.004)
- [30] Altuna A, Menendez de la Prida L, Bellistri E, Gabriel G, Guimerá A, Berganzo J, Villa R and Fernández L J 2012 SU-8 based microprobes with integrated planar electrodes for enhanced neural depth recording *Biosensors Bioelectron.* **37** 1–5
- [31] Coburn J C, Pottiger M T, Noe S C and Senturia S D 1994 Stress in polyimide coatings *J. Polym. Sci. B* **32** 1271–83
- [32] Kim B, Chen B, Gupta M and Meng E 2014 Formation of three-dimensional Parylene C structures via thermoforming *J. Micromech. Microeng.* **24** 065003
- [33] Wouters K and Puers R 2009 Determining the Young's modulus and creep effects in three different photo definable epoxies for MEMS applications *Sensors Actuators A* **156** 196–200
- [34] Kennedy P R 1989 The cone electrode: a long-term electrode that records from neurites grown onto its recording surface *J. Neurosci. Methods* **29** 181–93
- [35] Bartels J, Andreasen D, Ehirim P, Mao H, Seibert S, Wright E J and Kennedy P 2008 Neurotrophic electrode: method of assembly and implantation into human motor speech cortex *J. Neurosci. Methods* **174** 168–76
- [36] Brumberg J S, Nieto-Castanon A, Kennedy P R and Guenther F H 2010 Brain-computer interfaces for speech communication *Speech Commun.* **52** 367–79
- [37] Kim B J, Kuo J T W, Hara S A, Lee C D, Yu L, Gutierrez C A, Hoang T Q, Pikov V and Meng E 2013 3D Parylene sheath neural probe for chronic recordings *J. Neural Eng.* **10** 045002
- [38] Head B P, Hu Y, Finley J C, Saldana M D, Bonds J A, Miyanohara A, Niesman I R, Ali S S, Murray F and Insel P A 2011 Neuron-targeted caveolin-1 protein enhances signaling and promotes arborization of primary neurons *J. Biol. Chem.* **286** 33310–21
- [39] Petrossians A, Whalen J J III, Weiland J D and Mansfeld F 2011 Electrodeposition and characterization of thin-film platinum-iridium alloys for biological interfaces *J. Electrochem. Soc.* **158** D269–76
- [40] Sawyer D T 1974 Voltammetric indicator electrodes *Experimental Electrochemistry for Chemists* (New York: Wiley) pp 60–100
- [41] Felix S, Shah K, George D, Tolosa V, Tooker A, Sheth H, Delima T and Pannu S Removable silicon insertion stiffeners for neural probes using polyethylene glycol as a biodissolvable adhesive *Proc. Annual Int. Conf. of the IEEE Engineering in Medicine and Biology Society, EMBS* pp 871–4
- [42] Kozai T D Y and Kipke D R 2009 Insertion shuttle with carboxyl terminated self-assembled monolayer coatings for implanting flexible polymer neural probes in the brain *J. Neurosci. Methods* **184** 199–205
- [43] Chen Z-J, Gillies G T, Broaddus W C, Prabhu S S, Fillmore H, Mitchell R M, Corwin F D and Fatouros P P 2004 A realistic brain tissue phantom for intraparenchymal infusion studies *J. Neurosurg.* **101** 314–22
- [44] Pervin F and Chen W W 2011 Mechanically similar gel simulants for brain tissues *Dynamic Behavior of Materials* vol 1 (Berlin: Springer) pp 9–13
- [45] Kennedy P R, Mirra S S and Bakay R A E 1992 The cone electrode: ultrastructural studies following long-term recording in rat and monkey cortex *Neurosci. Lett.* **142** 89–94
- [46] Lein P J and Higgins D 1989 laminin and a basement-membrane extract have different effects on axonal and dendritic outgrowth from embryonic rat sympathetic neurons *in vitro Dev. Biol.* **136** 330–45
- [47] Kato Y, Saito I, Hoshino T, Suzuki T and Mabuchi K Preliminary study of multichannel flexible neural probes coated with hybrid biodegradable polymer *Eng. in Medicine and Biology Society, 2006. EMBS'06. 28th Annual Int. Conf. of the IEEE* 660-3
- [48] Winter J O, Cogan S F and Rizzo J F 2007 Neurotrophin-eluting hydrogel coatings for neural stimulating electrodes *J. Biomed. Mater. Res. B* **81** 551–63
- [49] Winter J O, Gokhale M, Jensen R J, Cogan S F and Rizzo J F 2008 Tissue engineering applied to the retinal prosthesis: neurotrophin-eluting polymeric hydrogel coatings *Mater. Sci. Eng. C* **28** 448–53
- [50] Noushi F, Richardson R T, Hardman J, Clark G and O'leary S 2005 Delivery of neurotrophin-3 to the cochlea using alginate beads *Otol. Neurotol.* **26** 528–33
- [51] Arth G E, Johnston D B, Fried J, Spooner W W, Hoff D R and Sarett L H 1958 16-Methylated steroids: I. 16 $\alpha$ -methylated analogs of cortisone, a new group of anti-inflammatory steroids *J. Am. Chem. Soc.* **80** 3160–1
- [52] Arth G E, Fried J, Johnston D B, Hoff D R, Sarett L H, Silber R H, Stoerk H C and Winter C A 1958 16-Methylated steroids: II. 16 $\alpha$ -methyl analogs of cortisone, a new group of anti-inflammatory steroids. 9 $\alpha$ -Halo derivatives *J. Am. Chem. Soc.* **80** 3161–3
- [53] Zhong Y, McConnell G, Ross J, DeWeerth S P and Bellamkonda R V 2005 A novel dexamethasone-releasing, anti-inflammatory coating for neural implants *2nd Int. IEEE EMBS Conf. on Neural Eng. (Arlington, VA)* 522-5
- [54] Mercanzini A, Reddy S, Velluto D, Colin P, Maillard A, Bensadoun J-C, Bertsch A, Hubbell J A and Renaud P 2007 Controlled release drug coatings on flexible neural probes

- 29th Annual Int. Conf. of the IEEE Engineering in Medicine and Biology Soc. (Lyon) 6612-5
- [55] Mercanzini A, Reddy S T, Velluto D, Colin P, Maillard A, Bensadoun J-C, Hubbell J A and Renaud P 2010 Controlled release nanoparticle-embedded coatings reduce the tissue reaction to neuroprostheses *J. Controlled Release* **145** 196–202
- [56] Shain W, Spataro L, Dilgen J, Haverstick K, Retterer S, Isaacson M, Saltzman M and Turner J N 2003 Controlling cellular reactive responses around neural prosthetic devices using peripheral and local intervention strategies *IEEE Trans. Neural Syst. Rehab. Eng.* **11** 186–8
- [57] Kim D-H and Martin D C 2006 Sustained release of dexamethasone from hydrophilic matrices using PLGA nanoparticles for neural drug delivery *Biomaterials* **27** 3031–7
- [58] Hara S A, Kim B J, Kuo J T W and Meng E 2015 An electrochemical investigation of the impact of microfabrication techniques on polymer-based microelectrode neural interfaces *J. Microelectromech. Syst.* **24** 801–9
- [59] Lee C D, Hara S A, Yu L, Kuo J T W, Kim B J, Hoang T, Pikov V and Meng E 2016 Matrigel coatings for Parylene sheath neural probes *J. Biomed. Mater. Res. B* **357–68**
- [60] Gibson S, Judy J W and Marković D 2010 Technology-aware algorithm design for neural spike detection, feature extraction, and dimensionality reduction *IEEE Trans. Neural Syst. Rehab. Eng.* **18** 469–78
- [61] Cogan S F 2008 Neural stimulation and recording electrodes *Annu. Rev. Biomed. Eng.* **10** 275–309